



## Less effective selection leads to larger genomes

Tristan Lefébure, Claire Morvan, Florian Malard, Clémentine François, Lara Konecny-Dupré, Laurent Guéguen, Michèle Weiss-Gayet, Andaine Seguin-Orlando, Luca Ermini, Clio Der Sarkissian, et al.

### ► To cite this version:

Tristan Lefébure, Claire Morvan, Florian Malard, Clémentine François, Lara Konecny-Dupré, et al.. Less effective selection leads to larger genomes. *Genome Research*, 2017, 27, pp.1016-1028. 10.1101/gr.212589.116 . hal-01544879v2

**HAL Id: hal-01544879**

**<https://inria.hal.science/hal-01544879v2>**

Submitted on 30 May 2017

**HAL** is a multi-disciplinary open access archive for the deposit and dissemination of scientific research documents, whether they are published or not. The documents may come from teaching and research institutions in France or abroad, or from public or private research centers.

L'archive ouverte pluridisciplinaire **HAL**, est destinée au dépôt et à la diffusion de documents scientifiques de niveau recherche, publiés ou non, émanant des établissements d'enseignement et de recherche français ou étrangers, des laboratoires publics ou privés.

# Less effective selection leads to larger genomes

Tristan Lefébure<sup>1</sup>, Claire Morvan<sup>1</sup>, Florian Malard<sup>1</sup>, Clémentine François<sup>1</sup>, Lara  
Konecny-Dupré<sup>1</sup>, Laurent Guéguen<sup>4</sup>, Michèle Weiss-Gayet<sup>2</sup>, Andaine  
Seguin-Orlando<sup>3</sup>, Luca Ermini<sup>3</sup>, Clio Der Sarkissian<sup>3</sup>, N. Pierre Charrier<sup>1</sup>, David  
5 Eme<sup>1</sup>, Florian Mermillod-Blondin<sup>1</sup>, Laurent Duret<sup>4</sup>, Cristina Vieira<sup>4,5</sup>, Ludovic  
Orlando<sup>3,6</sup>, and Christophe Jean Douady<sup>1,5</sup>

<sup>1</sup>Univ Lyon, Université Claude Bernard Lyon 1, CNRS UMR 5023, ENTPE, Laboratoire d'Ecologie des  
Hydrosystèmes Naturels et Anthropisés, F-69622 Villeurbanne, France

<sup>2</sup>Univ Lyon, Université Claude Bernard Lyon 1, CNRS UMR 5310, INSERM, Institut NeuroMyoGène,  
10 F-69622 Villeurbanne, France

<sup>3</sup>Center for GeoGenetics, Natural History Museum of Denmark, University of Copenhagen, Øster  
Voldgade 5-7, 1350K Copenhagen, Denmark

<sup>4</sup>Univ Lyon, Université Claude Bernard Lyon 1, CNRS UMR 5558, Laboratoire de Biométrie et Biologie  
Evolutive, F-69622 Villeurbanne, France

<sup>5</sup>Institut Universitaire de France, F-75005 Paris, France

<sup>6</sup>Université de Toulouse, University Paul Sabatier (UPS), CNRS UMR 5288, Laboratoire AMIS, F-31073  
Toulouse, France

March 23, 2017

**Corresponding author:** Tristan.Lefebure@univ-lyon1.fr

20 **Running title:** Less effective selection leads to larger genomes

**Keywords:** Genome size, effective population size, transposable elements, selection efficacy, Asel-  
lidae, groundwater

# Abstract

The evolutionary origin of the striking genome size variations found in eukaryotes remains enigmatic. The effective size of populations, by controlling selection efficacy, is expected to be a key parameter underlying genome size evolution. However, this hypothesis has proved difficult to investigate using empirical datasets. Here, we tested this hypothesis using twenty-two *de novo* transcriptomes and low-coverage genomes of asellid isopods, which represent eleven independent habitat shifts from surface water to resource-poor groundwater. We show that these habitat shifts are associated with higher transcriptome-wide  $d_N/d_S$ . After ruling out the role of positive selection and pseudogenization, we show that these transcriptome-wide  $d_N/d_S$  increases are the consequence of a reduction in selection efficacy imposed by the smaller effective population size of subterranean species. This reduction is paralleled by an important increase in genome size (25% increase on average), an increase also confirmed in subterranean decapods and mollusks. We also control for an adaptive impact of genome size on life history traits but find no correlation between body size, or growth rate, and genome size. We show instead that the independent increases in genome size measured in subterranean isopods are the direct consequence of increasing invasion rates by repeated elements, which are less efficiently purged out by purifying selection. Contrary to selection efficacy, polymorphism is not correlated to genome size. We propose that recent demographic fluctuations and the difficulty to observe polymorphism variations in polymorphism-poor species can obfuscate the link between effective population size and genome size when polymorphism data is used alone.

## Introduction

Eukaryotic organisms exhibit striking variations in their genome size (GS). Within animals, the range of GS extends from 20 Mb in the roundworm *Pratylenchus coffeae* to 130 Gb in the lungfish *Protopterus aethiopicus* (Gregory, 2005a). GS shows no correlation with organism complexity, an observation early referred to as the C-value paradox (Thomas, 1971). Even though the contribution of mechanisms such as polyploidization events or transposable element amplification to DNA gain or loss is now better understood (Gregory, 2005b), the evolutionary origin of GS variation still remains largely unexplained (Petrov, 2001).

Large genomes mostly consist of non-coding DNA (Gregory, 2005b; Lynch, 2007). The origins of the large variations in the amount of non-coding DNA found across eukaryotes are currently tentatively explained through two opposite sets of theories. Adaptive theories postulate that variation of the amount of non-coding DNA results in significant phenotypic changes and thus evolves under

the control of natural selection. Main examples of phenotypic changes commonly associated to GS  
 55 variations include nucleus and cellular sizes (Cavalier-Smith, 1982), growth rate (Grime and Mow-  
 forth, 1982) and metabolic rate (Vinogradov, 1995) variations. Conversely, non-adaptive theories  
 postulate that GS variations have little phenotypic impact (Doolittle and Sapienza, 1980), leaving  
 non-adaptive forces such as mutation and genetic drift as the main evolutionary drivers underlying  
 GS variation (Lynch and Conery, 2003). In particular, the mutational-hazard (MH) hypothesis sug-  
 60 gests that slightly deleterious mutations, including those that lead to GS variation, can segregate  
 in small populations where the efficacy of purifying selection is impaired by genetic drift (Lynch  
 et al., 2011; Lynch, 2011). Under this hypothesis, the evolution of GS would be controlled by the  
 balance between the emergence of large-scale insertions and deletions (indels) and their fixation  
 rate, which ultimately depends on the efficacy of selection and, thus, the effective population size  
 65 ( $N_e$ ).

Phylogenetic inertia, varying mutational patterns and uncertainties in  $N_e$  estimates, are but a  
 few difficulties that complicate testing of the MH hypothesis with empirical evidence. While GS  
 appears to correlate negatively with population size in eukaryotes (Lynch and Conery, 2003), in  
 agreement with the MH hypothesis, this relationship vanishes when accounting for phylogenetic  
 70 non-independence among taxa (Whitney and Garland, 2010). In addition, predictions of the MH  
 hypothesis can vary in opposite directions depending on the underlying pattern of indel mutations.  
 In eukaryotes, where indel mutation patterns are typically biased toward insertions, reductions  
 in population size are predicted to lead to increasing GS. Conversely, similar  $N_e$  reductions are  
 expected to result in decreasing GS in bacteria, for which the mutation pattern is biased toward  
 75 deletions (Kuo et al., 2009). Moreover, although essential to the MH hypothesis,  $N_e$  remains  
 difficult to estimate. Most studies rely on population polymorphism (Lynch and Conery, 2003) or  
 heterozygosity (Yi and Streelman, 2005), two measures that typically reflect population size history  
 over the last tens of thousands to millions of generations, while the pace of genome evolution might  
 take place at much longer temporal scales (Whitney and Garland, 2010; Whitney et al., 2011).

80 Since the formulation of the MH hypothesis, the few early empirical studies that originally  
 supported a relationship between GS and  $N_e$  (Lynch and Conery, 2003; Yi and Streelman, 2005)  
 have been criticized (Whitney and Garland, 2010; Gregory and Witt, 2008) and later analyses  
 failed to support this relationship. No relationships were found between GS and (i) allozyme  
 polymorphism in plants (Whitney et al., 2010), (ii) molecular polymorphism among different species  
 85 of rice (genus *Oryza*, Ai et al., 2012), and (iii) the relative population size in seed beetles (Arnqvist  
 et al., 2015), (iv) genetic drift in salamanders compared to frogs (Mohlhenrich and Mueller, 2016).

Finally, the influence of  $N_e$  on *Caenorhabditis* has been dismissed in favor of an adaptive explanation (Fierst et al., 2015). However, all these studies suffered either from the use of very indirect proxies of  $N_e$  or from small gene samples, often characterized for not more than 12 species (although  
 90 exceptions exist, see Whitney et al., 2010). Therefore, the influence of  $N_e$  on GS remains to be tested on an empirical dataset that provides a robust estimate of  $N_e$  within a statistically powerful framework.

Habitat shifts often result in drastic changes in population size and therefore offer useful case studies for testing the MH hypothesis. In this study, we use a comparative genomic approach to  
 95 test whether non-adaptive forces drive changes in GS following the habitat shift from surface water to groundwater within asellid isopods. The colonization of groundwater from surface water took place at multiple times and locations over the last tens to hundreds million years ago within this family (Morvan et al., 2013), thereby providing independent replicates of the transition to dark and low-energy habitats (Venarsky et al., 2014; Huntsman et al., 2011). Groundwater colonization  
 100 leads to eye-degeneration and is considered irreversible (Niemiller et al., 2013). We use 11 pairs of closely-related surface and subterranean asellid species to test the predictions of the MH hypothesis (Table S1). According to the MH hypothesis and assuming that consistent population size reduction took place following groundwater colonization, then, subterranean species are predicted to show reduced selection efficacy and larger GS than their surface relatives. We also considered alternative  
 105 hypotheses, namely (i) the possible reduction in GS in response to energy limitation in groundwater, and (ii) the selection of particular life history traits (hereafter, growth rate and body size) as a driver of patterns of GS variation.

## Results

### Efficacy of natural selection in groundwater

110 To evaluate differences in selection efficacy between surface and subterranean species, we sequenced and *de novo* assembled the transcriptomes of 11 pairs of asellid species. After gene families delimitation, we estimated the rate of non-synonymous over synonymous substitutions ( $d_N/d_S$ ) on a set of conserved and single copy genes. This ratio is jointly defined by the distribution of selection coefficient of new mutations ( $s$ ) and the magnitude of genetic drift as defined by  $N_e$  (Nielsen and  
 115 Yang, 2003). Therefore, the transcriptome-wide  $d_N/d_S$  is expected to increase over extended periods of small  $N_e$  because of the increasing fixation of slightly deleterious mutations (Ohta, 1992), an expectation confirmed in a wide range of animals (Galtier, 2016). Consequently, the transcriptome-

wide  $d_N/d_S$  is a direct proxy of selection efficacy. Subterranean species show significantly higher transcriptome-wide  $d_N/d_S$  than their surface relatives (Figure 1, Table 1). Looking at each pair of  
120 species independently, 8 pairs out of 11 display a higher subterranean transcriptome-wide  $d_N/d_S$ , a relative increase that can be as high as 59% (Figure 1).

While long periods of reduced  $N_e$  will induce higher transcriptome-wide  $d_N/d_S$ , adaptation to new habitats could potentially produce the same effect. Under the action of positive selection, beneficial non-synonymous mutations will reach fixation faster than their synonymous counterparts  
125 and will lead to sites with  $d_N/d_S > 1$ . If the frequency of such sites increases during the transition to groundwater, then, we can expect the transcriptome-wide  $d_N/d_S$  to increase. We first tested this adaptive hypothesis using a model that allows  $d_N/d_S$  variation across sites and makes it possible to differentiate between variation in the intensity of purifying ( $w^-$ ) and positive selection ( $w^+$ ) and their respective frequencies. Subterranean species do not show an elevated frequency ( $f(q(w^+))$ ) or  
130 intensity of positive selection ( $w^+$ ) but show higher  $w^-$  (Table 1 & S2, Figure S1 & S3). This supports a scenario in which subterranean species do not experience higher rates of positive selection, but instead evolve under reduced purifying selection efficacy.

We next tested the adaptive  $d_N/d_S$  increase scenario using polymorphism data. Under high rate of positive selection with recurrent fixation of non-synonymous mutations, populations will  
135 display an excess of non-synonymous substitutions compared to non-synonymous polymorphism (McDonald and Kreitman, 1991). We used the “direction of selection” statistics ( $DoS$ , Stoletzki and Eyre-Walker, 2011), which is a transcriptome-wide comparison of the rates of non-synonymous substitution and polymorphism, to test if positive selection indeed led to higher rates of fixation in subterranean species ( $DoS > 0$ ). Most subterranean species have negative  $DoS$  (Figure S4) and  
140 subterranean species do not have higher  $DoS$  than surface species (Table 1). On the contrary, in most species, irrespective of their habitat, the  $DoS$  is close to 0 or negative indicating that many slightly deleterious mutations are segregating in these species. While this observation is in line with the idea that effective population sizes reduces the efficacy of selection in these species, it does not completely rule out the hypothesis that subterranean species may have concomitantly evolved  
145 higher  $d_N/d_S$  as a result of more frequent adaptations during the shift from surface to subterranean habitats. When slightly deleterious mutations dominate the evolutionary dynamics, which appears to be the case in this group, they can mask the influence of adaptive evolution on polymorphism (James et al., 2016). We further tested this hypothesis by directly estimating the rate of adaptation ( $\alpha$ ) in two species pairs where subterranean species display elevated  $d_N/d_S$  than their surface sister  
150 species (*P. beticus* versus *P. jalionacus* and *P. coiffaiti* versus *P. cavaticus*, Figure 1). We used

a McDonald-Kreitman (McDonald and Kreitman, 1991) modified approach (Messer and Petrov, 2013) designed to cancel the influence of demography and linkage effects. For species such as the ones studied here, the high prevalence of segregating deleterious mutations at low frequency inflates the rate non-synonymous polymorphism and artificially decrease  $\alpha$  estimates. Messer and Petrov suggest to reconstruct  $\alpha$  as a function of the derived allele frequencies. As allele frequency increases, slightly deleterious alleles become rarer, to the point that a robust estimate of  $\alpha$  can be obtained by calculating the asymptotic  $\alpha$  for an allele frequency of 1. By re-sequencing the transcriptomes of 4 to 5 individuals per species, we reconstructed the unfolded site frequencies of these two pairs of species, fitted the distribution of  $\alpha(x)$  and estimated the asymptotic  $\alpha(1)$ . For each species we recovered the expected distribution of  $\alpha(x)$  as in Messer and Petrov (2013) and obtained asymptotic  $\alpha$  that were negative (Figure S5). While subterranean species of these two pairs of species show clear transcriptome-wide  $d_N/d_S$  increases, they do not display elevated rate of adaptation. For one pair there is no significant  $\alpha$  variation (*P. beticus* - *P. jalionacus*, p-value=0.49), while in the other pair the subterranean species shows lower  $\alpha$  estimates (*P. coiffaiti* - *P. cavaticus*, p-value=0.02). Therefore both *DoS* and  $\alpha$  analyses confirm that the increase in  $d_N/d_S$  in subterranean species is not caused by a higher rate of positive selection, in line with the results found on the model differentiating between variation in the intensity of purifying ( $w^-$ ) and positive selection ( $w^+$ ).

Subterranean species share multiple convergent regressive phenotypes, such as the loss of eyes and pigmentation which may ultimately be associated with gene non-functionalizations (Protas et al., 2005; Niemiller et al., 2013). A transcriptome-wide  $d_N/d_S$  increase can therefore also be caused by an excess of genes that have lost their function and consequently have acquired  $d_N/d_S$  nearing 1. As an example, the opsin gene of subterranean species has much higher  $d_N/d_S$  as a result of gene non-functionalization (see next section and Figure S6). Release of functional constraint on a gene and the resulting  $d_N/d_S$  increase should also be paralleled with much lower gene expression, if no expression at all (Zou et al., 2009; Yang et al., 2011). This is typically observed for the opsin gene that has much lower expression in the subterranean species (Figure S6). If gene non-functionalization in subterranean species is pervasive enough to shift the transcriptome-wide  $d_N/d_S$  upwards, we expect to see a subset of genes with lower expression in the subterranean species. We tested this hypothesis by comparing the expression of the genes in the surface and subterranean species of each pair. The set of conserved and single copy genes that was used to calculate each species  $d_N/d_S$  have much higher expression levels than the complete transcriptomes (Figure S7). This set of genes also displays more conserved gene expression levels across species (Figure S7). Finally, after counting changes in gene expression category between sister species, we found no

evidence of an excess of genes with lower expression in the subterranean species (Wilcoxon signed  
 185 rank test p-value=0.650, Table S4). We further tested this non-functionalization hypothesis by  
 looking for a subset of genes that would display larger  $d_N/d_S$  in the subterranean species while the  
 remaining genes would display no  $d_N/d_S$  variation. Distributions of the variation in gene  $d_N/d_S$   
 did not support the existence of such a small subset of genes (Figure S2). On the contrary, these  
 distributions were unimodal with a median positively correlated to the transcriptome-wide  $d_N/d_S$   
 190 ( $R^2 = 0.62$ , p-value = 0.004).

Altogether, we accumulated multiple evidences that the transcriptome-wide  $d_N/d_S$  increase  
 observed in subterranean species is not the consequence of increased levels of positive selection or  
 gene non-functionalization, but rather the result of convergent reductions in the efficacy of purifying  
 selection among subterranean species.

## 195 Polymorphism proxies of $N_e$

Instead of directly assessing selection efficacy, the MH hypothesis has traditionally been tested  
 using polymorphism data. Indeed, polymorphisms provide a direct proxy for  $N_e$ , which tunes the  
 magnitude of genetic drift and ultimately the efficacy of selection. As transcriptomes were sequenced  
 from pooled individuals, we estimated synonymous and non-synonymous polymorphism for genes  
 200 with high coverage. We used the population mutation rate ( $\hat{\theta}_w$ ) which is proportional to the product  
 of  $N_e$  and the mutation rate  $\mu$ , and the ratio of non-synonymous over synonymous polymorphism  
 ( $p_N/p_S$ ), which is expected to decrease with increasing  $N_e$ , independently of  $\mu$ . Both the  $d_N/d_S$   
 and the  $p_N/p_S$  measure the efficacy of selection to purge slightly deleterious mutations, though  
 the later works at a much shorter timescale. As expected,  $\hat{\theta}_w$  and  $p_N/p_S$  are negatively correlated  
 205 (phylogenetic generalized least-squares models, PGLS p-value <0.001,  $R^2 = 0.43$ ). Polymorphism  
 data are generally consistent with selection patterns inferred from  $d_N/d_S$ : subterranean species  
 have significantly higher  $p_N/p_S$  than their surface relatives in 6 out of 11 pairs, whereas there is  
 no pair significantly supporting the opposite pattern (Figure 1). However for  $\hat{\theta}_w$  the pattern is less  
 clear: in 6 pairs subterranean species have significantly lower  $\hat{\theta}_w$ , while in 3 pairs subterranean  
 210 species show significantly higher  $\hat{\theta}_w$  (Figure 1). Overall, the differences in  $p_N/p_S$  or  $\hat{\theta}_w$  between  
 subterranean and surface species are not statistically significant (Table 1). In addition, there is no  
 correlation between  $\hat{\theta}_w$  or  $p_N/p_S$  and the efficacy of selection as estimated using the transcriptome-  
 wide  $d_N/d_S$  (PGLS p-value=0.80 and 0.79, respectively). Traditional polymorphism proxies of  $N_e$   
 do not therefore support the same scenario as the one depicted using selection efficacy ( $d_N/d_S$ ).



## 215 Estimating colonization times with opsin sequences

Subterranean species may have colonized groundwater at different time periods, some being subterranean for a much longer time than others. Ignoring such differences through the use of a qualitative present-day ecological status (i.e. surface versus subterranean) may limit our power to detect a change in GS or polymorphism associated with the subterranean transition. One could contrast polymorphism measures and the time since the latest speciation event, where we know that a species ancestor was a surface species, but this would only be valid if speciation and colonization times were synchronous. Alternatively, we estimated the colonization time using the non-functionalization of the opsin gene. Indeed, similarly to observations made in underground mammals (Emerling and Springer, 2014), together with the regression of the ocular system, some subterranean species display loss-of-function mutations in eye pigment (Leys et al., 2005) or opsin genes (Niemiller et al., 2013), which are indicative of a loss of functional constraint. If we assume that opsin gene sequences have lost their function early in the process of groundwater colonization, then, they must have been evolving under a neutral model ( $d_N/d_S = 1$ ) since that colonization. Using a two states model of evolution with one surface opsin  $d_N/d_S$  estimated using opsins from surface species, and one subterranean opsin  $d_N/d_S$  equal to 1, we can then estimate the colonization time as a function of the speciation time and the estimated opsin  $d_N/d_S$  measured on a given branch leading to a subterranean species.

Using a combination of Sanger sequencing, transcriptome assemblies and genome sequencing reads, we reconstructed one opsin ortholog for 19 species out of 22. Irrespective of their ecological status, the two species of the genus *Bragasellus* probably do not possess this opsin locus. In addition, for one *Proasellus* subterranean species (*P. parvulus*), failure to amplify or recover Illumina reads from this locus suggests that the whole locus was lost in this species. Subterranean species showed lower opsin expression levels and had much higher opsin  $d_N/d_S$  ratios than surface species (average  $d_N/d_S = 0.3$  and  $0.05$ , respectively, Figure S6). In addition to one subterranean species which completely lost the loci (*P. parvulus*), two subterranean species also harbored clear non-functionalization signatures consisting of an 18 base-long deletion for *P. solanasi* and the insertion of a 280 base-long repeated element in the sequence of *P. cavaticus*. These observations validate the opsin locus as a colonization clock.

Estimated colonization times vary a lot with more than 50X variation between the youngest subterranean species (*P. jalionacus*, 2 MYA) and the oldest one (*P. herzegovinensis*, 122 MYA, Table S5). Colonization time is related to the regression of the eye and pigmentation, with species with intermediate phenotypes (reduced eyes and partial depigmentation) being very recent sub-

terranean species (Figure S8). Using relative colonization time ( $\frac{\text{time}_{\text{colonization}}}{\text{time}_{\text{speciation}}}$ ) for  $d_N/d_S$  ratios or absolute colonization time instead of the present-day ecological status gives very similar results (Table 1), indicating that variations in the colonization time are not likely to obfuscate polymorphism variations. Conversely, the strength of the correlation between the transcriptome-wide  $d_N/d_S$  (or  $w^-$ ) and relative colonization time is higher than with the ecological status (Table 1), reinforcing the hypothesis of a causal link between the subterranean colonization and the subsequent drop in selection efficacy. The only exception is the frequency of sites under positive selection ( $f_q(w^+)$ , Table 1) which becomes significantly higher in subterranean species when colonization time is used instead of ecological status (PGLS p-value=0.016, +0.6% per 100 MY of colonization).

## Genome size increase in groundwater

We next measured genome sizes in all 11 species pairs using flow cytometry. Using either the ecological status or the colonization time, we found a statistically significant increase in GS following the transition from surface to groundwater habitats (Figure 1, Table 1). Looking at each pair of species independently, 7 pairs out of 11 display a significantly higher GS, a relative increase reaching 137% in *P. hercegovinensis* (Figure 1). This finding is robust to the addition of 19 asellid species (PGLS with 41 asellids, p-value= 0.022, coefficient=0.273) and to the inclusion of a wider range of metazoans (linear mixed model with 18 independent pairs including Decapoda and Gastropoda, p-value = 0.040, 25% average increase in GS, Figure 2, Table S6).

## Linking genome size to selection efficacy

One of the main predictions of the MH hypothesis is that GS is negatively correlated with selection efficacy in eukaryotes. We validated this prediction because we found a highly significant positive relationship between GS and the transcriptome-wide  $d_N/d_S$  (or  $w^-$ , Table 1, Figure S9). In addition the  $d_N/d_S$  ratio (or  $w^-$ ) achieves similar, if not better, performance in predicting GS variation than the ecological status or colonization time (lower AIC and higher  $R^2$ , Table 1). When  $d_N/d_S$  (or  $w^-$ ) is put first and ecological status second into a single PGLS model of GS, the effect of the ecological status is no longer significant (PGLS p-value=0.189).

## Testing other covariates

In contradiction to the MH hypothesis, adaptative hypotheses postulate that variation in GS is under direct selection via its impacts on cellular (such as nucleus and cell sizes) and organismal

parameters (such as body size and growth rate) (Gregory, 2001). In many species, population size covaries with traits under selection such as growth rate and body size, themselves correlated to some extent to GS, making any causation test extremely challenging (Gregory, 2005b). While body size  
 280 was readily available in the literature, we estimated growth rate in 16 species using the RNA/protein ratio which is known to be positively correlated to growth rate in Rotifera (Wojewodzic et al., 2011). Indeed, in situ estimates of growth rates were out of reach, and a more traditional proxy such as the RNA/DNA ratio is inapplicable when GS varies. In accordance to the general assumption that subterranean animals tend to adopt K-selection life history traits, subterranean asellids species  
 285 display lower growth rate, though no trend was found regarding body size (Table 1). However, growth rate and body size do not correlate with GS (Table 1, Figure S9). Thus, although many forces might be at play during the transition to groundwater habitats, in asellids, we only found correlation between selection efficacy and GS.

## Mechanism of genome size increase

290 Implicit in the MH hypothesis is that an increase in GS should result from the progressive spread of insertions with slightly deleterious fitness effects, such as transposable elements (Vieira et al., 2002). Yet, other much faster mechanisms such as polyploidization events can also inflate GS (Otto, 2007). We tested for the occurrence of such large duplication events by looking for an excess of recent paralogs in the 11 subterranean species compared to their surface sister species. The mean  
 295 number of gene copy per gene family is not correlated to the ecological status nor to GS (PGLS  $p$ -value=0.773 and 0.579, respectively, Figure S10), indicating that subterranean species do not present an excess of recent duplication events.

To test for the accumulation of repeated elements, we evaluated the amount of repeated DNA in the 11 asellid species pairs using low-coverage genome sequencing, followed by clustering of the  
 300 highly repeated elements. Indeed, contrary to the non-repeated fraction of the genome, elements at high frequency will collect enough reads to be assembled. Summing across the contributions of each element provides an estimate for the size of the repeatome (ie. the fraction of the genome consisting of repeated DNA elements). We found larger repeatomes in large genomes (Figure 3A & D, Table 2, Figure S11). The repeatomes are largely made of repeat families found in a single species, called  
 305 repeat orphans, with very few shared repeats across species (Figure 3B). The occurrence of these shared repeats is largely explained by phylogenetic relatedness: closely related sister species share more than 200 repeat families with this number quickly decreasing with divergence time (Figure 3C). GS has little power to explain the composition of the repeatome. None of the axes of a repeatome

composition correspondence analysis is correlated to GS while the first three axes harbor a strong  
 310 phylogenetic signal (Blomberg  $K > 1$  with  $p\text{-value} < 0.01$ , Table S7, Figure S12).

The pattern of GS increase is globally congruent with a global increase of the repeatome inva-  
 siveness. Indeed, big genomes have at the same time more repeats and repeats at higher frequencies  
 (Table 2, Figure 3E & D). To a lesser extent, the number of repeat orphans and their frequencies  
 also increase with GS (Table 2), demonstrating that big genomes are also more prone to genome  
 315 invasion by new repeats. Nonetheless, the ratio of the total genomic size (TGS) occupied by new  
 repeats over common repeats do not change ( $\frac{TGS_{\text{orphans}}}{TGS_{\text{non-orphans}}}$ , Table 2), indicating that this aspect  
 of the repeat community structure does not change as GS increases. So, contrary to several model  
 organisms such as humans or maize, the GS increase was not induced by a very limited set of ele-  
 ments, but is the consequence of a repeat element community that became globally more invasive  
 320 subsequently to the ecological transition.

While the repeated portion of the genome increases linearly with GS, it does not explain 100%  
 of GS variations: on average 1Gb of repeats was gained for 1.3Gb of GS increase (Table 2). Con-  
 sequently, the estimated TGS of the non-repeated portion of the genome also increases with GS,  
 though at a much slower pace (1Gb for 2.8Gb, Table 2). Either repeats are harder to assemble  
 325 in large genomes or another minor mechanism is also at play during GS increase. Directly using  
 the repeatome size instead of GS in correlation analyses gives similar or reinforced results: while  
 polymorphism based  $N_e$  proxies ( $\hat{\theta}_w$  or  $p_N/p_S$ ), growth rate and body size do not correlate with  
 repeatome size, selection efficacy ( $d_N/d_S$  or  $w^-$ ) does (Table 1).

## Discussion

330 We found a substantial correlation between selection efficacy, as measured by transcriptome-wide  
 $d_N/d_S$ , and repeatome size. This finding indicates that, for a large part, GS is controlled by the  
 efficacy of selection to prevent the invasion of the genome by repeated elements. Conversely, we  
 found no correlation between  $N_e$  estimates derived from polymorphism data and GS. At first glance,  
 this result sounds contradictory since the efficacy of selection depends on  $N_e$ . We propose two non-  
 335 mutually exclusive hypotheses to explain this contradiction. First, while the transcriptome-wide  
 $d_N/d_S$  provides an average estimate of selection efficacy since the divergence of two species of a  
 pair, polymorphism-based proxies such as  $\hat{\theta}_w$  or  $p_N/p_S$  are influenced by recent  $N_e$  fluctuations,  
 independently of the divergence time. If  $N_e$  fluctuates rapidly with large amplitude around a  
 stable mean, polymorphism is likely to provide a noisy proxy of this mean, contrary to the  $d_N/d_S$ .

340 This hypothesis is supported by larger coefficients of variations for  $\hat{\theta}_w$  or  $p_N/p_S$  than for the  $d_N/d_S$   
 ( $CV_{d_N/d_S} = 0.22$ ,  $CV_{p_N/p_S} = 0.39$ ,  $CV_{\hat{\theta}_w} = 0.73$ , test of the equality of CVs p-value  $< 0.001$ ). In this  
 study, we observed the effect of multiple groundwater transitions that happened tens to hundreds  
 million years ago, a time scale long enough to produce large  $d_N/d_S$  and GS variations, but also  
 encompassing important climatic fluctuations which potentially generated shorter time-scale  $N_e$   
 345 variations. Particularly, quaternary climatic fluctuations are likely to have produced important  $N_e$   
 fluctuations in surface species which have much more unstable habitats than subterranean species.  
 Therefore, the lack of a clear correlation between short-term  $N_e$  proxies, like polymorphism, and  
 GS might be the consequence of recent climatic fluctuations. Interestingly, this hypothesis received  
 some support using Tajima's D tests. Indeed, only *P. beticus* (a surface species) out of the 4 species  
 350 for which we have adequate data to estimate Tajima's D is not at the mutation-drift equilibrium  
 (p-value=0.017, Table S8). This surface species shows evidence of recent population contraction  
 (Tajima's D  $> 0$ ) which might explain its unexpected combination of low polymorphism and low  
 $d_N/d_S$  when compared to its sister subterranean species (Figure 1). Second, polymorphism variation  
 might also be more prone to measurement artifacts than  $d_N/d_S$ . In particular, SNP calling errors  
 355 can constitute a relatively important fraction of detected variants among species with low levels of  
 polymorphism. For most species pairs (7 out of 11), we observed a higher level of polymorphism  
 in surface than in subterranean species (Figure 1, Figure S13). The four other cases all correspond  
 to pairs for which both species have low level of polymorphism, which might therefore be subject  
 to higher measurement error rates. This is in line with the strong relationship observed between  
 360 the surface species  $\hat{\theta}_w$  and the difference in  $\hat{\theta}_w$  between species pairs ( $R^2 = 0.74$ , p-value  $< 0.001$ ,  
 Figure S13). This suggests that below approximately 2‰,  $\hat{\theta}_w$  becomes a poor indicator of  $N_e$   
 changes. Altogether, the use of polymorphism proxies of  $N_e$  for polymorphism-poor species or for  
 species which experienced recent  $N_e$  variations might therefore result in misleading rejection of the  
 MH hypothesis.

365 Our findings shed new light on the debate of the validity of the MH hypothesis and the com-  
 parative methods that should be implemented to test it (Charlesworth and Barton, 2004; Gregory  
 and Witt, 2008; Whitney and Garland, 2010; Lynch, 2011; Whitney et al., 2011). Using a relatively  
 reduced set of ecologically-contrasted species pairs as true replicates of the same ecological transi-  
 tion is statistically more powerful than testing for differences in genomic attributes among a larger  
 370 set of distantly related taxa, in which the number of independent observations is unknown and for  
 which many traits varies. Accounting for phylogenetic effects in statistical analyses of GS variation  
 among multiple species is another yet crucial aspect because it increases not only specificity (Whit-

ney and Garland, 2010) but also sensitivity. Taken altogether, subterranean species do not have larger GS than surface species (ordinary least square linear model p-value = 0.122 for the 11 species pairs, p-value = 0.095 for the 41 asellid species, p-value = 0.261 for the 18 metazoan species pairs), whereas pairwise comparisons of surface and subterranean species (Figure 1 & 2) and PGLS models (Table 1) reveal a very clear and significant pattern of higher GS among subterranean species.

While there is several lines of evidence supporting a lower selection efficacy caused by long-term  $N_e$  reduction in subterranean species, we found little support that the colonization of this new habitat was also paralleled with adaptive evolution. The only evidence was found in the frequency of sites under positive selection when colonization time was used. The increase was nonetheless moderate (+0.6% per 100 MY of colonization) and was not supported by polymorphism ( $DoS$  or  $\alpha$ ) analyses. However, this study is limited to a small set of gene families that are found in most species, in a single copy and whose expression is very conserved. This set of genes is probably under strong purifying selection and might be less prone to positive selection. Fully investigating the relative role of adaptive versus non-adaptive forces during this ecological transition will require a much broader genomic approach.

Disentangling the forces that drive GS variation has commonly been complicated by rampant covariation between GS and multiple traits such as cell and body sizes, growth rates, metabolism and  $N_e$ , to name a few. In this study, we found no association between GS and two common covariates (body size and growth rate). While we cannot completely rule out other non-tested parameters and alternative ad hoc adaptive hypotheses, the results of this study are fully compatible and best explained by a causal relationship between  $N_e$  and GS. The mechanisms that drive genome size variation are also fully compatible with the MH hypotheses. The repeated elements were globally more diversified and more invasive in species with reduced selection efficacy, an expected outcome if selection against repeated element proliferation is less effective.

Documenting changes in the architecture of genomes among taxa that have undergone major shifts in habitats (Protas et al., 2005; Jones et al., 2012; Fang et al., 2014; Soria-Carrasco et al., 2014) holds much promise for disentangling evolutionary processes driving genome evolution. According with the MH hypothesis, our focus on the genomics of groundwater colonization brings new evidence for a prominent role of non-adaptive forces in GS evolution. Despite strong energetic constraints in groundwater, GS likely increases under the long-term effect of reduced  $N_e$ , which limits the strength of natural selection in hampering the invasion of slightly deleterious repeated elements. Altogether this study supports long-term effective population size variation as a key evolutionary regulator of genome features.

# Methods

## Aselloidea timetree

Phylogenetic comparative methods require accurate estimates of phylogenetic relationships and divergence times among species (Purvis et al., 1994). Both were inferred from a large timetree of Aselloidea containing 193 evolutionary units (Morvan et al., 2013) (Table S9). Sequences of the mitochondrial cytochrome oxidase subunit I (COI) gene, the 16S mitochondrial rDNA gene and the 28S nuclear rDNA gene used to build the Aselloidea timetree were obtained according to methods described in (Calvignac et al., 2011; Morvan et al., 2013). Alignments and Bayesian estimates of divergence times were conducted according to (Morvan et al., 2013). From the Aselloidea timetree, we selected 11 independent pairs of surface and subterranean asellid species as replicates of the ecological transition from surface water to groundwater.

## RNA-seq

For the 11 selected species pairs (Table S1) individuals were sampled from caves, springs, wells, and the hyporheic zone of streams using different pumping and filtering devices (Bou-Rouch pump, Cvetkov net, and Surber sampler) and were flash frozen alive. Total RNA was isolated using TRI Reagent (Molecular Research Center, Cincinnati, USA). Extraction quality was checked on a Bioanalyser RNA chip (Agilent Technologies, Santa Clara, USA) and RNA concentrations were estimated using a Qubit fluorometer (Thermo Fisher Scientific, Waltham, USA). Prior to any additional analysis, species identification was corroborated for each individual by sequencing a fragment of 16S gene. Equimolar pools of at least 5 individuals were made to achieve 10 µg of the total RNA (Table S1). Volumes were reduced using a Concentrator-Plus (Eppendorf, Hamburg, Germany) to achieve approximately 10 µL. Double strand poly(A)-enriched cDNA were then produced using the Mint2 kit (Evrogen, Moscow, Russia) following the manufacturer protocol except for the first-strand cDNA synthesis, where the CDS-1 adapter was used with the plugOligo-Adapter of the Mint1 kit (5'-AAGCAGTGGTATCAACGCAGAGTACGGGGG-P-3'). After sonication with a Bioruptor Nextgen UCD300 (Diagenode, Lige, Belgium) and purification with MinElute (Qiagen, Hilden, Germany), Illumina libraries were prepared using the NEBNext kit (New England BioLabs, Ipswich, USA) and amplified using 22 unique indexed primers. After purification with MinElute, 400-500 base pair fragments were size selected on an agarose gel. Libraries were paired-end sequenced on a HiSeq 2000 sequencer (Illumina, San Diego, USA) using 100 cycles at the Danish National High-throughput DNA Sequencing Center (Copenhagen, Denmark). A full lane was used for one species (*Proasellus beticus*), and

reads were resampled to represent about 2%, 5%, 10%, 25%, 50% and 100% of a full lane. These 6 sets of reads were *de novo* assembled (see next section) and the number of assembled components > 1kb was compared among sets (Figure S14). This preliminary experiment was used as a rational  
440 procedure to multiplex 4 species on one lane.

## Transcriptome assembly

Adapters were clipped from the sequence, low quality read ends were trimmed (phred score <30) and low quality reads were discarded (mean phred score <25 or if remaining length <19bp) using fastq-mcf of the ea-utils package (Aronesty, 2013). Transcriptomes were *de novo* assembled using  
445 Trinity (version 2013-02-25, Grabherr et al., 2011). Open reading frames (ORF) were identified with TransDecoder (<http://transdecoder.sourceforge.net/>). For each assembled component, only the longest ORF was retained, and gene families were delimited using all against all BLASTP (Altschul et al., 1990) and SiLiX (Miele et al., 2011). SiLiX parameters were set to i=0.6 and r=0.6 as they were maximizing the number of 1-to-1 orthologous gene families.

## $d_N/d_S$ calculation

Single copy orthologs were extracted for 3 different sets of taxa: the 11 asellid species pairs (320 genes), the ibero-aquitania clade (863 genes), and the alpine-coxalis clade (2257 genes) (see Figure 1). Each gene family was then aligned with the following procedure: (1) search and masking of frameshift using MACSE with frameshift cost set to -10 (Ranwez et al., 2011), (2) multiple align-  
455 ments of the translated sequences with PRANK (Löytynoja and Goldman, 2008) using the empirical codon model and F option, (3) site masking with Gblocks (Castresana, 2000) using -t=c, -b5=h and -b2 set as -b1. After gene concatenation, a transcriptome-wide  $d_N/d_S$  ratio was estimated with the free ratio model of CODEML from the package PAML 4.7a (Yang, 2007). Confidence intervals were obtained using 100 non-parametric bootstrap samples (random sampling of the codon sites  
460 with replacement).

To test whether the observed  $d_N/d_S$  increase could be attributed to a reduction in the efficacy of purifying selection or to an increase in positive selection (a higher number of sites under positive selection and/or an elevated positive selection intensity), we used the M10 branch-site model (Yang et al., 2000) as implemented in BppML (Dutheil and Boussau, 2008). To reduce computation times,  
465 the analysis was performed using quartets of taxa: the two species of a pair and two additional surface species used to root the tree. Large alignments (>300 000 codons) were reduced by randomly sampling 280 000 codons and only sites that were complete were retained. Purifying and positive



selection intensity ( $w^-$  and  $w^+$ ) and frequency ( $f q(w^-)$  and  $1 - f q(w^-)$ ) were estimated using the a posteriori mean site  $d_N/d_S$  using BppMixedLikelihoods (Dutheil and Boussau, 2008).

## 470 Single nucleotide polymorphism

Estimating population polymorphism from pooled RNA-seq samples is complicated by the fact that (1) RNA-seq is prone to both RT-PCR and sequencing errors (Gout et al., 2013), (2) polymorphism can be over-estimated by hidden paralogs (Gayral et al., 2013), and (3) it is difficult to differentiate low frequency alleles from sequencing errors in pooled data-sets (Futschik and Schlötterer, 2010).  
 475 While an accurate estimate is currently out of reach, it is possible to obtain polymorphism estimates that are comparable across taxa. We developed a statistical design that (1) is conservative in defining polymorphism, (2) balances the sampling effort so that estimates obtained within a species pair are comparable and (3) maximizes the number of analyzed genes to gain statistical power. Single nucleotide polymorphism (SNP) was searched on a set of 5027 gene families that were present  
 480 as a single copy in at least 6 out of the 11 species pairs. Gene families with hidden paralogs were filtered by using 10X coverage DNA-seq data available for 4 species (*P. karamani*, *P. hercegovinensis*, *P. ibericus* and *P. arthrodilus*). Gene families that had a DNA-seq coverage higher than the 90th percentile in any of these 4 species were filtered for any further polymorphism analysis. RNA-seq reads were aligned on the assembled ORF using BWA (aln algorithm, (Li and Durbin, 2009)).  
 485 SAMtools (Li et al., 2009) was then used to generate a BAM file, discard duplicated reads, and export a BCF file. SNPs were filtered and called with bcftools and vcutils.pl with the following conservative filtering parameters: minimum read depth of 10, minimum number of reads supporting an allele of 4, and minimum distance to a gap set to 15. Then, SNPs were classified as synonymous or non-synonymous. Only the genes that were highly covered in both species of a pair (average  
 490 coverage >50X, same results were obtained with lower coverage cutoff) were further considered to compute transcriptome-wide summary statistics (Table S3). This design ensured that synonymous and non-synonymous polymorphism estimates could be compared across taxa, although each of these estimates might be over or under estimated. We then calculated the population mutation rate ( $\theta$ ) using the Watterson estimator:

$$\hat{\theta}_w = \frac{p_S}{\sum_{i=1}^{2n-1} \frac{1}{i}}$$

495 with  $p_S$  the frequency of synonymous segregating sites and  $n$  the number of pooled individuals. Finally, we calculated the ratio of non-synonymous over synonymous segregating sites  $p_N/p_S$ . Con-

fidence intervals were obtained by bootstrapping the genes 10000 times.

This polymorphism data-set was also used to measure the direction of selection statistics (*DoS*, Stoletzki and Eyre-Walker, 2011) using:

$$DoS = \frac{D_n}{D_n + D_s} - \frac{P_n}{P_n + P_s}$$

500 with  $D_s$  and  $D_n$  the number of synonymous and non-synonymous divergences, and  $P_s$  and  $P_n$  the number of synonymous and non-synonymous polymorphisms. Divergences were measured with PAML 4.7a (Yang, 2007) and polymorphisms using the above described pipeline. *DoS* were measured gene by gene for every species pairs and compared for every pair using a wilcoxon signed rank test or globally using the median *DoS* per species.

## 505 Rate of adaptation and Tajima's D

For two species pairs (*P. beticus*, *P. jalionacus*, *P. coiffaiti* and *P. cavaticus*), we performed additional RNA-seq 50 base single-end Illumina sequencing, but this time by independently sequencing 4 to 5 individuals per species owing the estimation of allele frequencies. Reads were mapped on the assembled transcriptomes using BWA (mem algorithm, (Li and Durbin, 2009)), and SNPs were  
510 called using Reads2snp (Gayral et al., 2013). The site frequency spectrum (SFS) were then unfolded using the alignment with the respective sister species orthologs. Only sites with non-ambiguously reconstructed ancestral and derived allele were kept. We then used Messer and Petrov approach (Messer and Petrov, 2013) to directly estimate the proportion of adaptive substitutions ( $\alpha$ ) from the unfolded-SFS. Confidence intervals for  $\alpha$  were obtained by bootstrapping the SNP 1000 times.  
515 The same dataset was also used to test if population were at the mutation-drift equilibrium using Tajima's D test (Tajima, 1989).

## Colonization time

For 19 species, we were able to determine the sequence of one opsin gene. Sequences were determined using (i) transcriptome sequences, (ii) Sanger sequencing using (Taylor et al., 2005) PCR primers  
520 (LWF1a and Scylla) and PCR conditions, and (iii) genomic Illumina reads as detailed bellow. For the latter, reads were mapped on the closest available opsin sequence following the same approach as for the SNP search and a consensus was called with the Samtools program suite.

To estimate colonization time, we used the loss of function observed in several subterranean species and postulated that the opsin gene loss-of-function took place at the time of groundwater

525 colonization. We used a model with two  $d_N/d_S$  ratios, one for the functional opsins ( $\omega_{surf}$ ) and one for the non-functional opsin ( $\omega_1$ ) which was set to 1. We then defined the  $d_N/d_S$  of a branch leading to a subterranean taxa ( $\omega_{subt}$ ) as the weighted mean between these two defined ratios, such as:

$$\omega_{subt} = \omega_{surf} \frac{T-t}{T} + \omega_1 \frac{t}{T}$$

with  $T$  the speciation time, and  $t$  the time of colonization. From this, we estimated the time of  
530 colonization as follows:

$$t = T \times \frac{\omega_{subt} - \omega_{surf}}{1 - \omega_{surf}}$$

Another relevant parameter is the proportion of time a species has been subterranean since the divergence with its sister species, named the relative colonization time ( $RCT$ ), which we estimated using:

$$RCT = \frac{t}{T} = \frac{\omega_{subt} - \omega_{surf}}{1 - \omega_{surf}}$$

Opsin  $d_N/d_S$  were estimated using PAML free-ratio branch model, and the  $\omega_{surf}$  was estimated as  
535 the average  $d_N/d_S$  of the surface species showing the most obvious surface phenotypes (*P. coiffaiti*, *P. coxalis*, *P. karamani*, *P. ibericus*, *P. meridianus* and *P. beticus*).

## Measurement of genome size

We measured GS for 41 species of asellid (including the 11 species pairs), 4 Atyidae (Pancrustacea, Decapoda) and 2 Rissoidae (Mollusca, Gastropoda) (Table S6). After sampling, individuals were  
540 preserved at ambient temperature in silica gel. Measurements were conducted according to (Vieira et al., 2002). Nuclei were extracted from the head of organisms (or from entire individuals when body size was less than 3 mm in length). Heads were crushed in 200  $\mu$ L of cold modified Galbraiths nuclei isolation buffer (20 mM MOPS, 20.5 mM MgCl<sub>2</sub>, 35.5 mM trisodium citrate, 0.1% Triton X-100, 20  $\mu$ g mL<sup>-1</sup> boiled RNase A, pH 7.2 adjusted with NaOH; (Galbraith et al., 1983)). The  
545 mixture was filtered through 100  $\mu$ m and then 30  $\mu$ m mesh-size nets. The filtrate was centrifuged during 10 sec at 2600g and the supernatant was carefully removed. Pellets were resuspended in 200  $\mu$ L of nuclei isolation buffer. The resuspension was again centrifuged during 10 sec at 2600g and the supernatant was carefully removed. Pellets were resuspended in 250  $\mu$ L of buffer and transferred in 5 mL polystyrene round-bottom tubes. An amount of 50  $\mu$ L of propidium iodure was added to  
550 each tube. Tubes were kept in ice and darkness until GS measurements.

Genome sizes were measured using FACSCanto II flow cytometer (Becton Dickinson Instru-

ments) fitted with an argon laser at 488-nm wavelength. We analyzed 5 individuals per species. Individuals were measured in a random order and two individuals of the same species were never analyzed in the same run. Samples were calibrated to two external standards: *Drosophila virilis* females (GS of 0.41 pg, Bosco et al., 2007) and *Asellus aquaticus* (GS of 2.49 pg, Rocchi et al., 1988, and authors' cross validation). The *Drosophila* were maintained under laboratory conditions at 25 °C for two to three generations before GS measurements. Standards were prepared using the protocol described above from 5 organism heads and were measured in each run (2 measures for *D. virilis* at the beginning and end of runs and 5 measures for *A. aquaticus* evenly distributed during the runs).

The FlowQ bioconductor package (Gentleman et al., 2004) in R software (R Core Team, 2013) was used for quality assessment of flow cytometry data. All the flow cytometer analyses were checked for cell number, boundary events and time anomalies. Cell subsetting known as gating, was firstly performed manually using the BD FACSDiva software (BD Biosciences). Secondly, the automatic curvHDR filtering method (Naumann et al., 2010) was used to select the cells located in the highest density region (HDR level = 0.8). Then, when drift over time was significant, gated values were corrected using a linear regression on *A. aquaticus* reference using the following equation:  $IP_{corr} = IP_x - \frac{IP_x}{IP_{st}} \times (x - x_0) \times \lambda$ , where  $IP_{corr}$  is the corrected gated value,  $IP_x$  is the gated value to correct,  $IP_{st}$  is the *A. aquaticus* reference gated value at the beginning of the run (time  $t = x_0$ ) estimated by the linear regression,  $x$  is the measurement time for the gated value to correct,  $x_0$  is the time at the beginning of the run and  $\lambda$  is the slope of the linear regression on *A. aquaticus* reference. Drift was considered significant when the regression on *A. aquaticus* reference had adjusted  $R^2$  values  $\geq 0.1$ . Finally, GS were derived from fluorescence data using *D. virilis* as a standard for Asellidae and Rissoidae and using *A. aquaticus* as a standard for Attyidae. Indeed, large GS in Attyidae (previously known GS range from 3.30 to 7.20 pg, Gregory, 2005a) prevented the use of *D. virilis* as a standard.

## Growth rate and body size

Growth rates were estimated using the total RNA normalized by the total protein biomass of an organism (RNA/protein ratio, Wojewodzic et al., 2011) for at least 7 individuals per species. Total RNA and proteins were isolated using TRI Reagent (Molecular Research Center). RNA concentrations were calculated by fluorometry with a Qubit (Life Technologies). Total proteins were obtained using the Bicinchoninic acid assay (Smith et al., 1985). Body size were estimated using maximum body size as reported in each species description.

## Genome sequencing

585 To compare the size of the repeatome between surface and subterranean species, we sequenced the genome of the 11 pairs of Asellidae species. For 4 species (*P. ibericus*, *P. arthrodilus*, *P. karamani*, *P. hercegovinensis*), we built blunt-ended libraries for shotgun sequencing on Illumina platforms, as described in (Orlando et al., 2013; Seguin-Orlando et al., 2013) with few modifications. One  $\mu\text{g}$  of DNA in 100  $\mu\text{L}$  TE buffer was sheared using a Bioruptor NGS device (Diagenode) with four cycles  
590 of 15 seconds ON/90 seconds OFF. The obtained size distributions of sheared DNA fragments were centered at around 500 bp. After concentration in 22  $\mu\text{L}$  EB buffer (Qiagen) with the MinElute PCR Purification kit (QIAGEN), the sheared DNA fragments were built into blunt-ended DNA libraries using the NEBNext Quick DNA Library Prep Master Mix Set for 454 (New England BioLabs, reference nb. E6070L), following the protocol described in (Meyer and Kircher, 2010),  
595 but with 0.5  $\mu\text{M}$  Illumina adapters (final concentration). All reactions were carried out in 25  $\mu\text{L}$  volumes; incubation times and temperatures were as follows: 20 min at 12°C, 15 min at 37°C for end-repair; 20 min at 20°C for ligation; 20 min at 37°C, 20 min at 80°C for fill-in. After the end-repair and ligation steps, reaction mixes were purified using the MinElute PCR Purification Kit (Qiagen) using elution volumes of 16  $\mu\text{L}$  and 22  $\mu\text{L}$  of EB buffer, respectively. The final 25  $\mu\text{L}$   
600 volume of blunt-end libraries was split in two parts and PCR amplified independently in 50  $\mu\text{L}$  reaction mixes containing: 5 units Taq Gold (Life Technologies), 1X Gold Buffer, 4 mM  $\text{MgCl}_2$ , 1 mg/ml BSA, 0.25 mM of each dNTP, 0.5  $\mu\text{M}$  of Primer inPE1.0 (5'-AAT GAT ACG GCG ACC ACC GAG ATC TAC ACT CTT TCC CTA CAC GAC GCT CTT CCG ATC T-3) and 0.5  $\mu\text{M}$  of an Illumina 6 bp-indexed (I) primer (5-CAA GCA GAA GAC GGC ATA CGA GAT III III GTG ACT GGA GTT CAG ACG TGT GCT CTT CCG-3). Thermocycling conditions for  
605 the amplifications were: activation at 92°C for 10 min; followed by nine cycles of denaturation at 92°C for 30 sec, annealing at 60°C for 30 sec, elongation at 72°C for 30 sec; and final elongation at 72°C for 7 min. PCR products were purified using the MinElute PCR Purification kit, with a final elution volume of 25  $\mu\text{L}$  EB buffer.

For the remaining 18 species, we built Illumina TruSeq DNA PCR-free LT libraries (Illumina, catalog FC-121-3001), following manufacturers recommendations. Briefly, 1  $\mu\text{g}$  of DNA extract  
610 was sheared in a total volume of 50  $\mu\text{L}$  TE buffer, using a Bioruptor NGS device (Diagenode) with three cycles of 25 seconds ON/90 seconds OFF. The fragmented DNA was cleaned up using Illumina Sample Purification Beads. After end-repair, the DNA fragments were size-selected around 350bp using two consecutive bead purification steps, A-tailed, and ligated to 6bp-indexed Illumina TruSeq  
615 adaptors (Set A). Two last bead purifications were performed to remove any adaptor dimer and the final libraries were resuspended in a volume of 20  $\mu\text{L}$  Resuspension Buffer. In order to control

for contaminations, library and PCR blanks were carried out at the same time as the samples. Amplified libraries and blanks were quantified using the 2100 Bioanalyzer (Agilent) High-Sensitivity DNA Assay. No detectable amount of DNA could be recovered from the blanks. Blunt-End indexed  
 620 DNA libraries were pooled and sequenced on two lanes of a HiSeq 2000 Illumina platform (100 cycles paired-end mode run), while the two PCR-free libraries pools were sequenced each on one flow-cell of the Hiseq 2500 Illumina platform (150 paired-end run, Rapid Mode, 6bp index read), at the Danish National High-Throughput DNA Sequencing Centre.

## Repeatome size estimates

625 We used low coverage read sequencing to characterize repeated genome sequences (Novák et al., 2010) using RepeatExplorer (Novák et al., 2013). Prior to analysis, DNA-seq reads were randomly sampled to achieve 0.05X coverage following the GS estimated by flow cytometry, so that estimates are comparable across taxa. After clustering of the reads into highly repeated elements by RepeatExplorer, the number of reads representing each repeated element is a direct function of the  
 630 repeat frequency, the GS, and the sequencing effort. The proportion of the genome (GP) made by this repeat is  $GP_i = n_{reads_i} / n_{reads}$ , with  $n_{reads_i}$  the number of reads making the repeat  $i$ , and  $n_{reads}$  the total number of reads. The proportion of genome made of repeats (the repeatome size) is then  $GP = \sum_i GP_i$ . By default, RepeatExplorer filters repeat elements that have genome proportion lower than 0.01%. To achieve comparable estimates independent of genome sizes, the  
 635 number of repeats or the repeatome size of a given genome were recalculated by filtering repeats that occupied less than 0.5 Mb. A repeat element total genomic size (TGS) was then calculated as  $TGS_i = GP_i \times GS_j$  with  $GS_j$  the genome size of species  $j$ . Repeat families were delimited using blastn (e-value=0.1) and SiLiX (i=50 and r=70).

## Comparative analyses

640 Phylogenetic generalized least squares (PGLS) regression models (Martins and Hansen, 1997) were used to test for the correlation between 2 variables. We first tested the association between the ecological transition and population size, biological traits or GS (top of Table 1). PGLS were also used to test for the association between GS and population size, biological traits (bottom of Table 1) or genomic features (Table 2). The correlation between two variables was assessed by comparing a  
 645 model without the predictor variable (intercept model) to a model including the predictor variable using a likelihood ratio test (LRT). Analyses were performed in R using ape (Paradis et al., 2004) and nlme (Pinheiro et al., 2014) packages. The best model of trait evolution and its associated

covariance structure, in our case the Brownian motion model, was selected according to minimum Akaike information criterion (AIC). The difference in  $\hat{\theta}_w$ ,  $p_N/p_S$ , and  $d_N/d_S$  between the two species of a surface - subterranean pair was tested using the proportion of bootstrap replicates supporting a difference (critical level = 5%) and the difference in GS was tested using a Wilcoxon rank sum test with 5 measurements of GS (ie. 5 individuals) per species. We also performed ordinary least squares models to test for the effect of the ecological status on GS while ignoring phylogenetic relationships among species. To test for the effect of the ecological transition on GS using a wider range of taxa (ie. 18 species pairs including Decapoda and Mollusca with 5 measurements of GS per species), we performed a linear mixed model in R using the nlme package because a chronogram with accurate branch length could not be obtained given the available molecular markers and calibration points. The ecological status (ie. surface versus subterranean) was a fixed effect, and we specified the random error structure as ecological status nested into species pairs to account for phylogenetic relationships among species. Then, we performed the model with no hierarchy in the random error structure, which is equivalent to an ordinary least squares model, to test for the effect of the ecological status on GS while ignoring phylogenetic relationships among species. Differences in the coefficient of variations of different variables were tested using modified signed-likelihood ratio test (Krishnamoorthy and Lee, 2014) using the R package cvequality.

## Data access

Sequence reads and assemblies have been deposited to the European Nucleotide Archive (ENA; <http://www.ebi.ac.uk/ena>) under the study accession number PRJEB14193. Sanger sequences were submitted to NCBI (GenBank; <https://www.ncbi.nlm.nih.gov/nucleotide/>) under the accession numbers KC610091-KC610505 (Table S9).

## Acknowledgments

This work was supported by the Agence Nationale de la Recherche (ANR-08-JCJC-0120-01 DEEP, ANR-15-CE32-0005 Convergenomix); the Institut Universitaire de France; the European Commission (7th EU Framework Programme, Contract No. 226874, BioFresh), the CNRS (APEGE No. 70632, PEPS ExoMod 2014 and Enviromics 2014), the french embassy in Denmark, the Danish National Research Foundation (DNRF94) and the Marie-Curie Intra-European Fellowship (IEF 302617). We thank the following collaborators and organizations for their help in collecting biolog-

ical material: Alhama de Granada municipality, Besson JP, Bodon M, Bouillon M, Capderrey C, Carreira I, Chatelier B, Colson-Proch C, Creuzé des Chatelliers M, Cueva de Valporquero, Culver D, Datry T, Delegacion provincial de medio ambiente Ronda, Ferrandini J, Ferrandini M, Fiser C, Fong D, Gina D, Gottstein S, Gouffre de Padirac, Kaufmann B, Knight L, Lana E, Le Pennec R, Lescher-Moutoue F, Magniez G, Messana G, Michel G, Nassar E, Nassar-Simon N, Notenboom J, Orozco R, Parc National du Mercantour, Parco Naturale Alta Valle Pesio e Tanaro, Planes S, Prié V, Reboleira AS, Sauve municipality, Sendra A, Simon L, Sket B, Stoch F, Turjak M and Zigmajster M. We thank the laboratory technicians at the Danish High-throughput DNA Sequencing Centre for technical assistance. We thank Boulesteix M, Burley N, Goubert C, Paradis E and Simon L for providing advices on the analyses, Biémont C and Schaack S for their advices or comments on earlier drafts of this manuscript. We gratefully acknowledge support from the CNRS/IN2P3 Computing Center (Lyon/Villeurbanne - France), for providing a significant amount of the computing resources needed for this work. This work was performed using the computing facilities of the CC LBBE/PRABI. We thank 2 anonymous reviewers and Adam Eyre-Walker for their comments.

## Disclosure declaration

The authors declare no conflicts of interest.

## References

- Ai B, Wang ZS, and Ge S. 2012. Genome size is not correlated with effective population size in the oryza species. *Evolution* **66**: 3302–3310.
- Altschul SF, Gish W, Miller W, Myers EW, and Lipman DJ. 1990. Basic local alignment search tool. *J. Mol. Biol.* **215**: 403–410.
- Arnqvist G, Sayadi A, Immonen E, Hotzy C, Rankin D, Tuda M, Hjelman CE, and Johnston JS. 2015. Genome size correlates with reproductive fitness in seed beetles. *Proc. R. Soc. Lond., B, Biol. Sci.* **282**: 20151421.
- Aronesty E. 2013. Comparison of sequencing utility programs. *Open Bioinformatics Journal* **7**: 1–8.
- Bosco G, Campbell P, Leiva-Neto JT, and Markow TA. 2007. Analysis of drosophila species genome size and satellite dna content reveals significant differences among strains as well as between species. *Genetics* **177**: 1277–1290.
- Calvignac S, Konecny L, Malard F, and Douady CJ. 2011. Preventing the pollution of mitochondrial datasets with nuclear mitochondrial paralogs (numts). *Mitochondrion* **11**: 246–254.
- Castresana J. 2000. Selection of conserved blocks from multiple alignments for their use in phylogenetic analysis. *Mol. Biol. Evol.* **17**: 540–552.
- Cavalier-Smith T. 1982. Skeletal dna and the evolution of genome size. *Annu. Rev. Biophys. Bioeng.* **11**: 273–302.
- Charlesworth B and Barton N. 2004. Genome size: does bigger mean worse? *Curr. Biol.* **14**: R233–R235.
- Doolittle WF and Sapienza C. 1980. Selfish genes, the phenotype paradigm and genome evolution. *Nature* **284**: 601–603.
- Dutheil J and Boussau B. 2008. Non-homogeneous models of sequence evolution in the bio++ suite of libraries and programs. *BMC Evol. Biol.* **8**: 255.
- Emerling CA and Springer MS. 2014. Eyes underground: regression of visual protein networks in subterranean mammals. *Mol. Phylogenet. Evol.* **78**: 260–270.
- Fang X, Nevo E, Han L, Levanon EY, Zhao J, Avivi A, Larkin D, Jiang X, Feranchuk S, Zhu Y, et al. 2014. Genome-wide adaptive complexes to underground stresses in blind mole rats spalax. *Nat. Commun.* **5**: 10.1038/ncomms4966.
- Fierst JL, Willis JH, Thomas CG, Wang W, Reynolds RM, Ahearne TE, Cutter AD, and Phillips PC. 2015. Reproductive mode and the evolution of genome size and structure in caenorhabditis nematodes. *PLoS Genet.* **11**: e1005323.



- Futschik A and Schlötterer C. 2010. The next generation of molecular markers from massively parallel sequencing of pooled dna samples. *Genetics* **186**: 207–218.
- Galbraith DW, Harkins KR, Maddox JM, Ayres NM, Sharma DP, and Firoozabady E. 1983. Rapid flow cytometric analysis of the cell cycle in intact plant tissues. *Science* **220**: 1049–1051.
- Galtier N. 2016. Adaptive protein evolution in animals and the effective population size hypothesis. *PLoS Genet.* **12**: 1–23.
- Gayral P, Melo-Ferreira J, Glémin S, Bierne N, Carneiro M, Nabholz B, Lourenco JM, Alves PC, Ballenghien M, Faivre N, et al.. 2013. Reference-free population genomics from next-generation transcriptome data and the vertebrate-invertebrate gap. *PLoS Genet.* **9**: e1003457.
- Gentleman RC, Carey VJ, Bates DM, Bolstad B, Detting M, Dudoit S, Ellis B, Gautier L, Ge Y, Gentry J, et al.. 2004. Bioconductor: open software development for computational biology and bioinformatics. *Genome Biol.* **5**: R80.
- Gout JF, Thomas WK, Smith Z, Okamoto K, and Lynch M. 2013. Large-scale detection of in vivo transcription errors. *Proc. Natl. Acad. Sci. U.S.A.* **110**: 18584–18589.
- Grabherr MG, Haas BJ, Yassour M, Levin JZ, Thompson DA, Amit I, Adiconis X, Fan L, Raychowdhury R, Zeng Q, et al.. 2011. Full-length transcriptome assembly from RNA-Seq data without a reference genome. *Nat. Biotechnol.* **29**: 644–652.
- Gregory TR. 2001. Coincidence, coevolution, or causation? dna content, cellsize, and the c-value enigma. *Biological Reviews* **76**: 65–101.
- Gregory TR. 2005a. Animal genome size database. <http://www.genomesize.com>.
- Gregory TR. 2005b. *The evolution of the genome*. Elsevier, San Diego.
- Gregory TR and Witt JD. 2008. Population size and genome size in fishes: a closer look. *Genome* **51**: 309–313.
- Grime J and Mowforth M. 1982. Variation in genome size – an ecological interpretation. *Nature* **299**: 151–153.
- Huntsman BM, Venarsky MP, Benstead JP, and Huryn AD. 2011. Effects of organic matter availability on the life history and production of a top vertebrate predator (plethodontidae: Gyrinophilus palleucus) in two cave streams. *Freshwat. Biol.* **56**: 1746–1760.
- James JE, Piganeau G, and Eyre-Walker A. 2016. The rate of adaptive evolution in animal mitochondria. *Mol. Ecol.* **25**: 67–78.
- Jones FC, Grabherr MG, Chan YF, Russell P, Mauceli E, Johnson J, Swofford R, Pirun M, Zody MC, White S, et al.. 2012. The genomic basis of adaptive evolution in threespine sticklebacks. *Nature* **484**: 55–61.
- Krishnamoorthy K and Lee M. 2014. Improved tests for the equality of normal coefficients of variation. *Computational Statistics* **29**: 215–232.
- Kuo CH, Moran NA, and Ochman H. 2009. The consequences of genetic drift for bacterial genome complexity. *Genome Res.* **19**: 1450–1454.
- Leys R, Cooper SJ, Strecker U, and Wilkens H. 2005. Regressive evolution of an eye pigment gene in independently evolved eyeless subterranean diving beetles. *Biol. Lett.* **1**: 496–499.
- Li H and Durbin R. 2009. Fast and accurate short read alignment with burrows-wheeler transform. *Bioinformatics* **25**: 1754–1760.
- Li H, Handsaker B, Wysoker A, Fennell T, Ruan J, Homer N, Marth G, Abecasis G, Durbin R, et al.. 2009. The sequence alignment/map format and samtools. *Bioinformatics* **25**: 2078–2079.
- Löytynoja A and Goldman N. 2008. Phylogeny-aware gap placement prevents errors in sequence alignment and evolutionary analysis. *Science* **320**: 1632–1635.
- Lynch M. 2007. *The origins of genome architecture*, volume 98. Sinauer, Sunderland.
- Lynch M. 2011. Statistical inference on the mechanisms of genome evolution. *PLoS Genet.* **7**: e1001389.
- Lynch M, Bobay LM, Catania F, Gout JF, and Rho M. 2011. The repatterning of eukaryotic genomes by random genetic drift. *Annu. Rev. Genomics Hum. Genet.* **12**: 347–366.
- Lynch M and Conery JS. 2003. The origins of genome complexity. *Science* **302**: 1401–1404.
- Martins EP and Hansen TF. 1997. Phylogenies and the comparative method: a general approach to incorporating phylogenetic information into the analysis of interspecific data. *Am. Nat.* pp. 646–667.
- McDonald JH and Kreitman M. 1991. Adaptive protein evolution at the Adh locus in *Drosophila*. *Nature* **351**: 652–654.
- Messer PW and Petrov DA. 2013. Frequent adaptation and the mcdonald-kreitman test. *Proc. Natl. Acad. Sci. U.S.A.* **110**: 8615–8620.
- Meyer M and Kircher M. 2010. Illumina sequencing library preparation for highly multiplexed target capture and sequencing. *Cold Spring Harbor Protocols* **2010**: pdb.prot5448.
- Miele V, Penel S, and Duret L. 2011. Ultra-fast sequence clustering from similarity networks with SiLiX. *BMC Bioinformatics* **12**: 116.
- Mohlhenrich ER and Mueller RL. 2016. Genetic drift and mutational hazard in the evolution of salamander genomic gigantism. *Evolution* **70**: 2865–2878.
- Morvan C, Malard F, Paradis E, Lefébure T, Konecny-Dupré L, and Douady C. 2013. Timetree of aselloidea reveals species diversification dynamics in groundwater. *Syst. Biol.* **62**: 512–522.
- Naumann U, Luta G, and Wand MP. 2010. The curvhdr method for gating flow cytometry samples. *BMC Bioinformatics* **11**: 44.

- Nielsen R and Yang Z. 2003. Estimating the distribution of selection coefficients from phylogenetic data with applications to mitochondrial and viral dna. *Mol. Biol. Evol.* **20**: 1231–1239.
- Niemiller ML, Fitzpatrick BM, Shah P, Schmitz L, and Near TJ. 2013. Evidence for repeated loss of selective constraint in rhodopsin of amblyopsid cavefishes (teleostei: Amblyopsidae). *Evolution* **67**: 732–748.
- Novák P, Neumann P, and Macas J. 2010. Graph-based clustering and characterization of repetitive sequences in next-generation sequencing data. *BMC Bioinformatics* **11**: 378.
- Novák P, Neumann P, Pech J, Steinhaisl J, and Macas J. 2013. Repeatexplorer: a galaxy-based web server for genome-wide characterization of eukaryotic repetitive elements from next-generation sequence reads. *Bioinformatics* **29**: 792–793.
- Ohta T. 1992. The nearly neutral theory of molecular evolution. *Annu. Rev. Ecol. Syst.* **23**: 263–286.
- Orlando L, Ginolhac A, Zhang G, Froese D, Albrechtsen A, Stiller M, Schubert M, Cappellini E, Petersen B, Moltke I, et al.. 2013. Recalibrating equus evolution using the genome sequence of an early middle pleistocene horse. *Nature* **499**: 74–78.
- Otto SP. 2007. The evolutionary consequences of polyploidy. *Cell* **131**: 452–462.
- Paradis E, Claude J, and Strimmer K. 2004. APE: analyses of phylogenetics and evolution in R language. *Bioinformatics* **20**: 289–290.
- Petrov DA. 2001. Evolution of genome size: new approaches to an old problem. *Trends Genet.* **17**: 23–28.
- Pinheiro J, Bates D, DebRoy S, Sarkar D, and R Core Team. 2014. *nlme: Linear and Nonlinear Mixed Effects Models*. R package version 3.1-117.
- Protas ME, Hersey C, Kochanek D, Zhou Y, Wilkens H, Jeffery WR, Zon LI, Borowsky R, and Tabin CJ. 2005. Genetic analysis of cavefish reveals molecular convergence in the evolution of albinism. *Nat. Genet.* **38**: 107–111.
- Purvis A, Gittleman JL, and Luh HK. 1994. Truth or consequences: effects of phylogenetic accuracy on two comparative methods. *J. Theor. Biol.* **167**: 293–300.
- R Core Team. 2013. *R: A Language and Environment for Statistical Computing*. R Foundation for Statistical Computing, Vienna, Austria.
- Ranwez V, Harispe S, Delsuc F, and Douzery EJ. 2011. MACSE: Multiple alignment of coding sequences accounting for frameshifts and stop codons. *PLoS ONE* **6**: e22594.
- Rocchi A, Lanza V, and Di Castro M. 1988. Surface spreading of synaptonemal complexes in three isopod crustacean species. *Genetica* **78**: 125–132.
- Seguin-Orlando A, Schubert M, Clary J, Stagegaard J, Alberdi MT, Prado JL, Prieto A, Willerslev E, and Orlando L. 2013. Ligation bias in illumina next-generation dna libraries: implications for sequencing ancient genomes. *PLoS ONE* **8**: e78575.
- Smith P, Krohn RI, Hermanson G, Mallia A, Gartner F, Provenzano M, Fujimoto E, Goeke N, Olson B, and Klenk D. 1985. Measurement of protein using bicinchoninic acid. *Anal. Biochem.* **150**: 76–85.
- Soria-Carrasco V, Gompert Z, Comeault AA, Farkas TE, Parchman TL, Johnston JS, Buerkle CA, Feder JL, Bast J, Schwander T, et al.. 2014. Stick insect genomes reveal natural selections role in parallel speciation. *Science* **344**: 738–742.
- Stoletzki N and Eyre-Walker A. 2011. Estimation of the neutrality index. *Mol. Biol. Evol.* **28**: 63–70.
- Tajima F. 1989. Statistical method for testing the neutral mutation hypothesis by dna polymorphism. *Genetics* **123**: 585–595.
- Taylor SD, de la Cruz KD, Porter ML, and Whiting MF. 2005. Characterization of the long-wavelength opsin from mecoptera and siphonaptera: does a flea see? *Mol. Biol. Evol.* **22**: 1165–1174.
- Thomas C. 1971. The genetic organization of chromosomes. *Annu. Rev. Genet.* **5**: 237–256.
- Venarsky MP, Huntsman BM, Huryn AD, Benstead JP, and Kuhajda BR. 2014. Quantitative food web analysis supports the energy-limitation hypothesis in cave stream ecosystems. *Oecologia* **176**: 859–869.
- Vieira C, Nardon C, Arpin C, Lepetit D, and Biémont C. 2002. Evolution of genome size in drosophila. is the invader's genome being invaded by transposable elements? *Mol. Biol. Evol.* **19**: 1154–1161.
- Vinogradov AE. 1995. Nucleotypic effect in homeotherms: body-mass-corrected basal metabolic rate of mammals is related to genome size. *Evolution* **49**: 1249–1259.
- Whitney KD, Baack EJ, Hamrick JL, Godt MJW, Barringer BC, Bennett MD, Eckert CG, Goodwillie C, Kalisz S, Leitch IJ, et al.. 2010. A role for nonadaptive processes in plant genome size evolution? *Evolution* **64**: 2097–2109.
- Whitney KD, Boussau B, Baack EJ, and Garland T. 2011. Drift and genome complexity revisited. *PLoS Genet.* **7**: e1002092.
- Whitney KD and Garland T. 2010. Did genetic drift drive increases in genome complexity? *PLoS Genet.* **6**: e1001080.
- Wojewodziec MW, Rachamim T, Andersen T, Leinaas HP, and Hessen DO. 2011. Effect of temperature and dietary elemental composition on rna/protein ratio in a rotifer. *Functional Ecology* **25**: 1154–1160.
- Yang L, Takuno S, Waters ER, and Gaut BS. 2011. Lowly expressed genes in arabidopsis thaliana bear the signature of possible pseudogenization by promoter degradation. *Mol. Biol. Evol.* **28**: 1193–1203.
- Yang Z. 2007. PAML 4: phylogenetic analysis by maximum likelihood. *Mol. Biol. Evol.* **24**: 1586–1591.
- Yang Z, Nielsen R, Goldman N, and Pedersen AMK. 2000. Codon-substitution models for heterogeneous selection pressure at amino acid sites. *Genetics* **155**: 431–449.

- Yi S and Streelman JT. 2005. Genome size is negatively correlated with effective population size in ray-finned fish. *Trends Genet.* **21**: 643–646.
- Zou C, Lehti-Shiu MD, Thibaud-Nissen F, Prakash T, Buell CR, and Shiu SH. 2009. Evolutionary and expression signatures of pseudogenes in arabidopsis and rice. *Plant Physiol.* **151**: 3–15.

# Figures

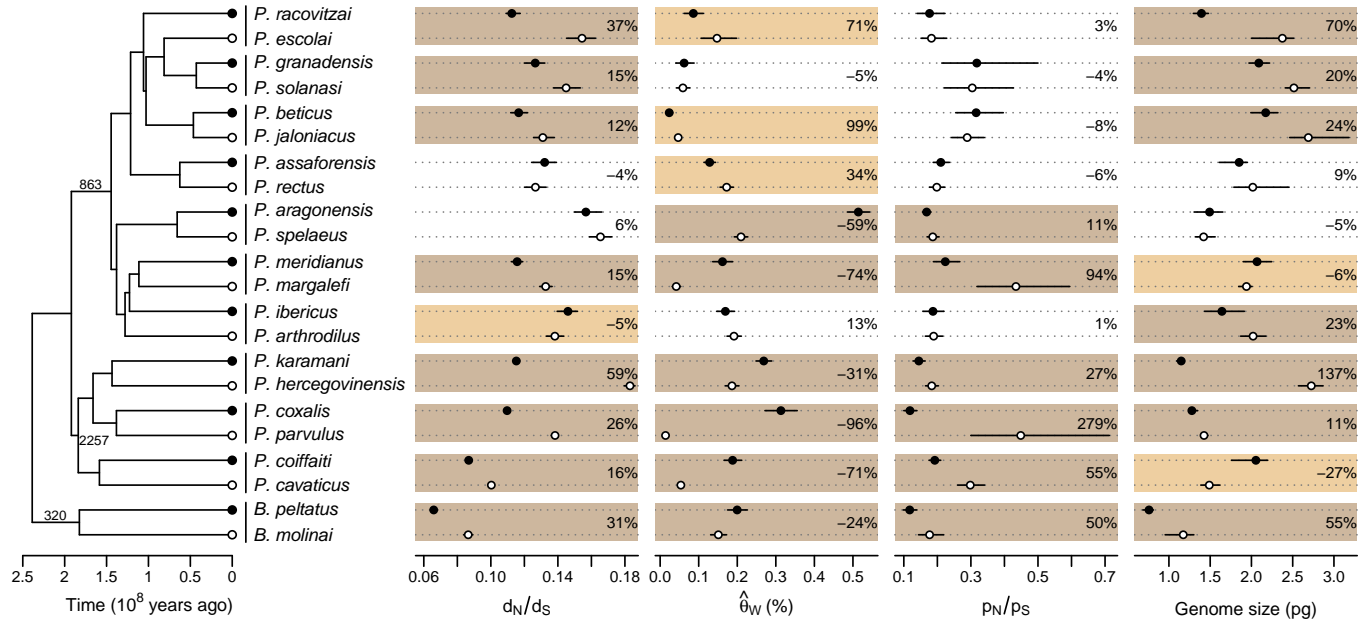


Figure 1:

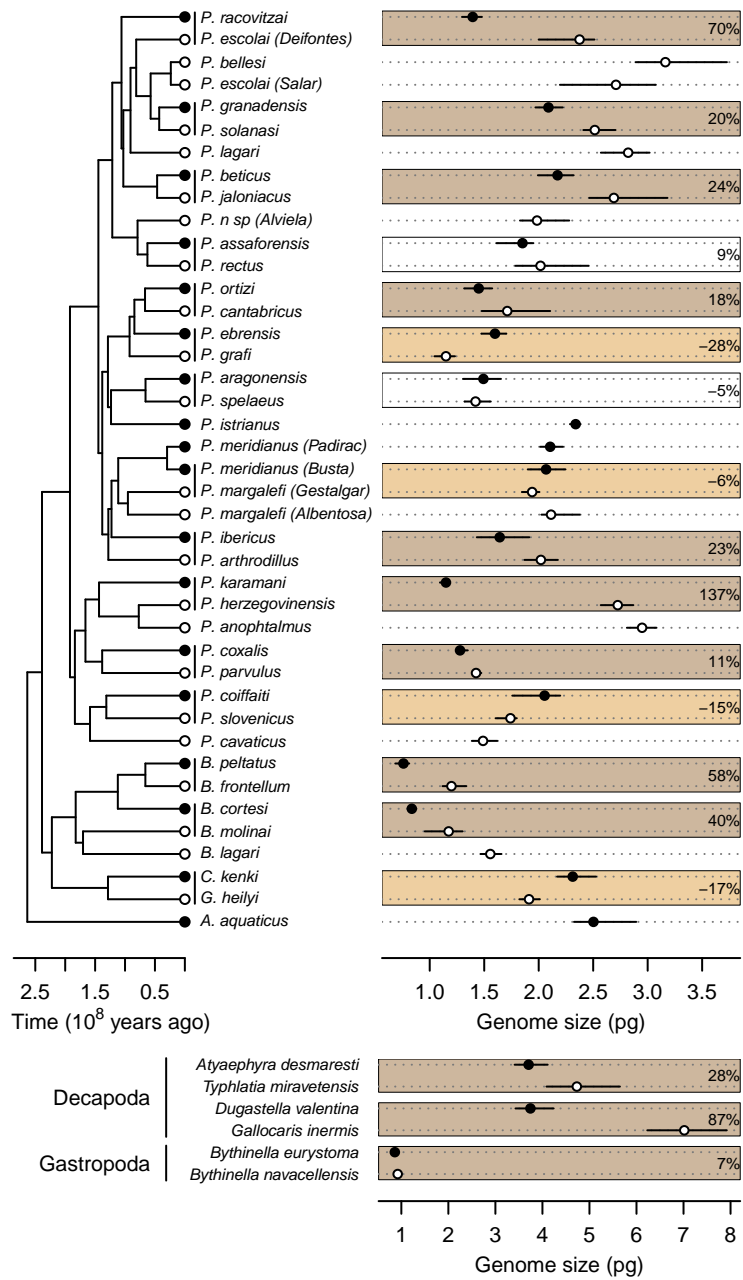


Figure 2:

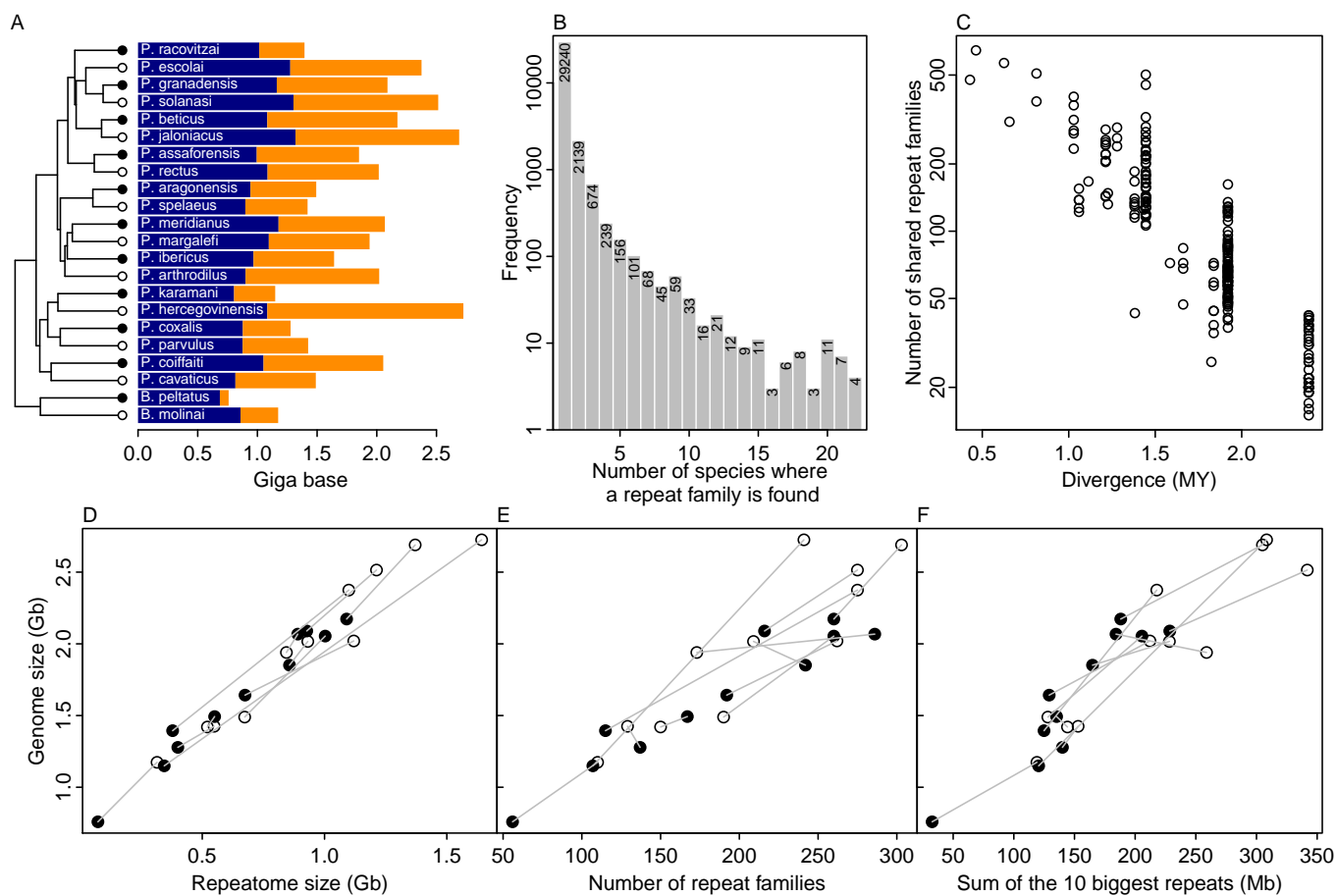


Figure 3:

## Figure legends

**Figure 1** Selection efficacy ( $d_N/d_S$ ), polymorphism ( $\hat{\theta}_w$  and  $p_N/p_S$ ) and haploid genome size measurements for 11 pairs of surface and subterranean asellid species. Vertical bars next to the tree indicate species pairs with their surface (black circles) and subterranean (white circles) species. Numbers along branches of the tree are the numbers of single copy genes used to estimate the  $d_N/d_S$ . Color boxes indicate statistical support (p-value<0.05) in favor of (dark brown) or against (light brown) a decrease in selection efficacy or population size, or an increase in genome size in subterranean species. No box indicates no statistical differences between species of a pair. Error bars represent 95% bootstrap confidence intervals, except for genome size where it represents the range around the mean for 5 individuals. The percentage change from surface water to subterranean species is shown for each species pair.

**Figure 2** Variation in haploid genome size associated with the ecological transition from surface water to groundwater in 47 species, including isopods (top panel), decapods and gastropods (bottom panel). The 18 independent pairs of surface and subterranean species are delimited with boxes. Legends as in Figure 1. Identical species names followed by locality names within brackets refer to cryptic species (Morvan et al., 2013).

**Figure 3** Repeatome size estimates and composition using low coverage genome sequencing. A: size of the non-repeated genome (blue) and repeatome (orange) for the 22 species (tree symbols as in figure 1). B: Repeat family frequency spectrum. C: Number of shared repeats between two species as a function of divergence time. Relationship between GS and repeatome size (D), the number of repeat families (E) and the total genomic size of the 10 biggest repeat families (F). In the panel D, E and F, surface (black circles) and subterranean (white circles) species of a pair are joined by a grey line.

## Tables

Table 1: Phylogenetic generalized least squares (PGLS) models testing the correlation between two variables. On the top of the table, correlation tests between the transition to groundwater (ecological status, proportion of subterranean branch, or colonization time) and variables ranging from selection efficacy ( $d_N/d_S$ ,  $w^-$ ), rate of adaptive evolution ( $w^+$ ,  $fq(w^+)$ ,  $DoS$ ), polymorphism ( $\hat{\theta}_w$  and  $p_N/p_S$ ), and phenotypic traits (growth rate and body size) are reported. Another set of correlation tests between GS, or repeatome size, and some of these variables is also reported at the bottom of the table. Coefficients are in contrast to the surface status. Only comparable AIC are shown (same dependent variable and same number of observations).  $w^-$ : intensity of purifying selection,  $w^+$ : intensity of positive selection,  $fq(w^+)$ : frequency of sites under positive selection,  $DoS$ : direction of selection, LRT p-value: likelihood ratio test between the models with and without the given predictor variable.  $R^2$ : Cox and Snell generalized  $R^2$ . n: number of observations. \*: p-value < 0.05, \*\*: p-value < 0.01. The relative colonization time represents the proportion of the terminal branches estimated to be subterranean using the opsin gene, it is equal to  $\text{time}_{\text{colonization}}/\text{time}_{\text{speciation}}$ .

Dependent variable	Predictor variable	n	LRT p-value	Coefficient	AIC	$R^2$
$d_N/d_S$	ecological status	22	0.015*	0.017		0.237
$w_-$		22	0.020*	0.018		0.217
$w^+$		22	0.355	-0.197		0.038
$fq(w^+)$		22	0.653	0.001		0.009
$DoS$		22	0.410	0.056		0.030
$\hat{\theta}_w$		22	0.099	-0.001		0.117
$p_N/p_S$		22	0.232	0.036		0.063
growth rate		16	0.011*	-6.211		0.332
body size		22	0.192	-1.135		0.074
$d_N/d_S$	relative colonization time	19	0.001**	0.064		0.427
$w_-$		19	0.001**	0.073		0.420
$w^+$		19	0.521	-0.465		0.021
$fq(w^+)$	colonization time	19	0.016*	0.006		0.263
$DoS$		19	0.817	0.035		0.003
$\hat{\theta}_w$		19	0.486	-0.001		0.025
$p_N/p_S$		19	0.355	0.058		0.044
growth rate		13	0.115	-7.813		0.174
body size		19	0.581	-1.134		0.016
Genome size	ecological status	22	0.014*	0.340	29.1	0.240
	colonization time	19	0.019*	0.789		0.250
	$d_N/d_S$	22	0.009**	10.447	28.3	0.266
	$w^-$	22	0.004**	9.897	26.8	0.315
	$\hat{\theta}_w$	22	0.450	-64.920	34.6	0.026
	$p_N/p_S$	22	0.428	0.823	37.8	0.028
	growth rate	16	0.178	-0.022		0.107
	body size	22	0.862	0.006	35.1	0.001
Repeatome size	ecological status	22	0.017*	0.251	29.1	0.229
	colonization time	19	0.003**	0.724		0.372
	$d_N/d_S$	22	0.006**	8.189	15.3	0.287
	$w^-$	22	0.002**	7.808	13.5	0.344
	$\hat{\theta}_w$	22	0.437	-50.457	22.2	0.027
	$p_N/p_S$	22	0.419	0.633	22.1	0.029
	growth rate	16	0.148	-0.017		0.123
	body size	22	0.916	0.003	22.8	0.001



Table 2: Phylogenetic generalized least squares models testing the association between genome size (dependent variable) and the size and composition of the 22 species repeatomes. Same abbreviation as in Table 1, TGS: total genomic size, Gb: giga base, top1: most invasive repeat, orphan: repeat element found in one species only.

Predictor variable	LRT p-value	Coefficient	AIC	R <sup>2</sup>
repeatome size (Gb)	<.0001***	1.295	-33.0	0.955
non-repeated genome size (Gb)	<.0001***	2.773	6.5	0.728
number of repeats	<.0001***	0.007	3.7	0.760
top1 TGS (Gb)	0.0022***	20.546	25.7	0.348
top10 TGS (Gb)	<.0001***	5.407	1.6	0.783
repeat orphans TGS (Gb)	0.0163*	0.002	29.4	0.231
number of orphan repeats	0.0056**	0.003	27.5	0.294
orphans TGS / non-orphans TGS	0.3797	-0.203	34.4	0.034